RESEARCH ARTICLE

Recombinant Human Collagen-Based Bioinks for the 3D Bioprinting of Full-thickness Human Skin Equivalent

Yang Yang[1,2,3†], Runze Xu[1,2,3†], Chengjin Wang[1,2,3], Yuzhi Guo[1,2,3], Wei Sun[1,2,3,4*], Liliang Ouyang[1,2,3*]

[1]Department of Mechanical Engineering, Tsinghua University, Beijing 100084, China
[2]Biomanufacturing and Rapid Forming Technology Key Laboratory of Beijing, Tsinghua University, Beijing 100084, China
[3]Biomanufacturing and Engineering Living Systems – Innovation International Talents Base (111 Base), Tsinghua University, Beijing 100084, China
[4]Department of Mechanical Engineering and Mechanics, Drexel University, Philadelphia, PA 19104, USA
[†]*These authors contribute equally to this work*

Abstract: As a major extracellular matrix component within the skin, collagen has been widely used to engineer human skin tissues. However, most collagen is extracted from animals. Here, we introduced recombinant human type III collagen (rhCol3) as a bioactive component to formulate bioinks for the bioprinting of a full-thickness human skin equivalent. Human dermal fibroblasts were encapsulated in the gelatin methacryloyl-rhCol3 composite bioinks and printed on a transwell to form the dermis layer, on which human epidermal keratinocytes were seeded to perform an air-liquid interface culture for 6 weeks. After optimizing the bioink formulation and bioprinting process, we investigated the effect of rhCol3 on skin tissue formation. The results suggest that a higher concentration of rhCol3 would enhance the growth of both cells, resulting in a more confluent (~100%) spreading of the epidermal keratinocytes at an early stage (3 days), compared to the rhCol3-free counterpart. Moreover, in an *in vivo* experiment, adding rhCol3 in the hydrogel formulation would contribute to the skin wound healing process. Taken together, we conclude that rhCol3 could act as a functional bioink component to promote basic skin cellular processes for skin tissue engineering.

Keywords: Recombinant human collagen; Skin constructs; 3D printing; Bioinks

***Correspondence to:** Liliang Ouyang, Department of Mechanical Engineering, Tsinghua University, Beijing 100084, China; ouy@tsinghua.edu.cn; Wei Sun, Department of Mechanical Engineering, Tsinghua University, Beijing 100084, China; weisun@tsinghua.edu.cn

Received: May 6, 2022; **Accepted:** June 5, 2022; **Published Online:** August 25, 2022

(This article belongs to the *Special Issue: Composite/Multi-component Biomaterial Inks and Bioinks*)

Citation: Yang Y, Xu R, Wang C, *et al*., 2022. Recombinant Human Collagen-Based Bioinks for the 3D Bioprinting of Full-thickness Human Skin Equivalent. *Int J Bioprint*, 8(4): 611. Doi: http://doi.org/10.18063/ijb.v8i4.611

1. Introduction

Skin is the largest organ of the human body that functions as a physical barrier to protect inner organs from physical contact, toxins, pathogens, and loss of heat and water[1]. The skin tissue is composed of the epidermis and its underlying dermis. The maintenance of the epidermis integrity is regulated through a balance between proliferation and differentiation of the residing epidermal cells, mostly epidermal keratinocytes[2]. The dermis, primarily composed of dermal fibroblasts, could interact with epidermal keratinocytes through biochemical cues (e.g., keratinocytes growth factor) and hence regulate epidermis growth[3].

The skin extracellular matrix (ECM) is an another significant part of the skin stem cell niche that supports the adhesion, migration, proliferation, and differentiation of skin cells, which are fundamental cellular processes for skin tissue development and regeneration[4]. Type I and type III collagens are the major structural constituents of ECM in native skin[5]. Particularly, type III collagen was

found to be critical in dermal collagen fibrillogenesis and tissue integrity. Meanwhile, type III collagen has been shown to induce the transcription of growth factors for fibroblasts, including keratin growth factor, vimentin, and transforming growth factor beta (TGF-β)[6-8]. The content and the ratio of these two types of collagens were found to vary with age and injury. For instance, the type III collagen in normal fetal skin accounts for approximately 34 – 65% of the total collagen, while later in the childhood and early adult life, approximately 80 – 85% of the collagen in the skin are type I[9-12]. Meanwhile, the content ratio of type III collagen in the skin hypertrophic scar tissue was found to be from 14% to 28%[13]. This content change with time has been inferred to be involved in skin ECM remodeling, in support of the fact that skin tissue architecture is highly dynamic and heterogeneous[10,14]. The previous studies have indicated that both epidermal cells and fibroblasts are sensitive to attached or embedded substrate with various physical cues, for instance, stiffness[15]. The integrin-binding motifs decorated to the matrices surface have also shown to bind epithelial progenitors and further promote their migration and wound healing. For instance, human skin fibroblasts with mutated type III collagen gene were unable to organize collagens and fibronectin in the ECM due to the downregulation of α2β1 integrin[8,16].

Thus, it is desirable to recapitulate the dynamic and heterogeneous human skin tissue microenvironment when engineering *in vitro* skin tissue for either pharmaceutical or regenerative applications. The previous studies have engineered *in vitro* three-dimensional (3D) human skin equivalents based on human skin cells, which are both structurally and functionally more similar to native human skin than 2D culture models and animal models[17,18]. This field is greatly advanced by the use of innovative biofabrication technologies, such as 3D bioprinting, in which 3D skin tissue could be pre-designed and then precisely fabricated following layer-by-layer assembling of cell-laden bioinks to yield spatial heterogeneity[19]. Laser-assisted, inkjet-based, and extrusion-based bioprinting are three major techniques used for the fabrication of skin equivalents. For instance, Lee *et al.* fabricated 3D skin tissue through inkjet printing multilayer constructs[20], and Koch *et al.* utilized laser-assisted bioprinting to build *in vitro* skin tissue in predefined patterns[21]. Some groups have obtained 3D-printed human skin equivalents using naturally derived biomaterials, such as collagen I, to resemble ECM environment[22]. Nonetheless, efforts are still required to improve mimicking complex human skin tissue microenvironment of the *in vitro* skin equivalent. For instance, the effect of significant type III collagen on skin formation is poorly understood as it has been rarely involved in the engineering of *in vitro* human skin models. Moreover, the typically formulated bioinks based on collagen usually lack proper printability due to the slow gelation kinetics at physiological conditions.

To address these problems, we propose to formulate recombinant human type III collagen (rhCol3) into bioinks for the bioprinting of a full-thickness human tissue equivalent. In general, recombinant human collagens have been designed and synthesized as alternative biomaterials to the native human collagen, with the advantages of high purity, batch-to-batch consistency, and low immunogenicity[23]. Moreover, they have been reported to support cellular activities[24], being applied to the engineering of bone and neural tissues[25]. Recently, a biomaterial composed by gelatin and recombinant type III collagen has been proven to support the growth of seeded NIH-3T3 cells and promote the regeneration of damaged rat skin[26]. Herein, we hypothesize that rhCol3 has an important role in supporting human skin cell growth and hence would facilitate the formation of the epidermis *in vitro* and wound healing *in vivo* since native human type III collagen is the second abundant ECM structural collagen in the skin[27]. To achieve printing convenience, we formulated a composite bioink by mixing rhCol3 with gelatin methacryloyl (GelMA), a commonly used printable biomaterial[28]. To model the contents of type III collagen in native human skin tissues (**Figure 1A**)[11,29], we developed the composite bioinks with varied rhCol3 contents ranging from 0.8 to 3.2 wt%, representing 10 – 30% ratio of matrix polymer in the bioinks. We optimized the bioprinting of this novel bioink formulation based on rheological and printability assessments. Then, we constructed an *in vitro* 3D human skin equivalent with human epidermal keratinocytes (HaCaTs) and dermal fibroblasts (HDF) using extrusion-based 3D bioprinting. Basically, the rhCol3-based bioink formulations consisting of base component GelMA, bioactive rhCol3, and photoinitiator (lithium phenyl-2,4,6-trimethylbenzoylphosphinate, LAP) were prepared at the predefined concentration (**Figure 1B**). Then, we fabricated the dermal constructs by 3D bioprinting of HDF-laden bioinks followed by photocrosslinking (**Figure 1C**). After 3 days of culture, the constructed dermal layers were seeded with HaCaTs on top (**Figure 1D**) followed by submerging culture to allow for HaCaTs and HDFs proliferation (**Figure 1E**). An air-liquid interface (ALI) culturing method was performed to obtain the differentiated epidermal layers (**Figure 1F**). Based on this skin model, we comprehensively investigated the effects of rhCol3 on the cellular processes of skin cells *in vitro*. We also assessed the skin repair process based on *in vivo* analysis of implanting GelMA-rhCol3 hydrogel onto Sprague Dawley (SD) rat dorsal wound (**Figure 1G**). Collectively, both *in vitro* skin construct and *in vivo* wound healing analysis indicated that

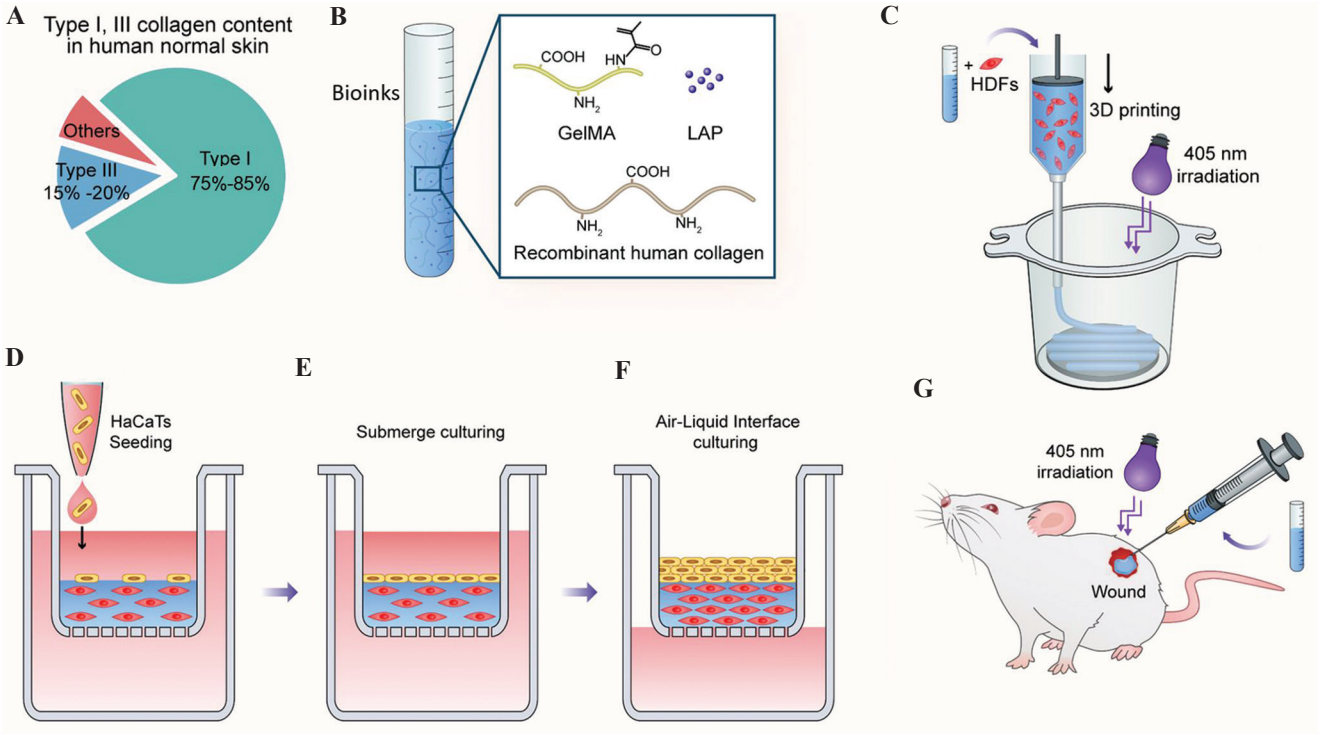

Figure 1. Schematic illustration of constructing the *in vitro* skin equivalent using rhCol3-based bioinks and 3D bioprinting, together with an *in vivo* test. (A) The content of type I and III collagen to the total collagens presented in the human skin. (B) Preparation of the rhCol3-based bioink formulations consisting of base component GelMA, bioactive rhCol3, and photoinitiator LAP. (C) 3D bioprinting of the HDFs-laden dermal constructs on a transwell followed by photocrosslinking. (D) Seeding of HaCaTs on top of printed dermal constructs. (E) Submerge culturing of the *in vitro* 3D skin tissue. (F) Air-liquid interface culturing process to obtain the differentiated epidermal layer. (G) *In vivo* test of the biocompatibility of the GelMA-rhCol3 bioinks.

GelMA-rhCol3 mimicked skin tissue microenvironment that supports skin cell adhesion, migration, proliferation, and differentiation, which are critical processes involved in skin repair and regeneration.

2. Materials and methods

2.1. Preparation of GelMA and GelMA-rhCol3 bioinks

GelMA solutions at concentrations of 5, 7.5, and 10 wt% were prepared by fully dissolving the GelMA powder (SunP Gel-G1, degree of substitution 55 – 65%, porcine skin, 300 g bloom, SunP Biotech) in Dulbecco's phosphate-buffered saline (Wisent, Canada) that contains 0.25 wt% lithium phenyl-2,4,6-trimethylbenzoylphosphinate (LAP, SunP Biotech) as photoinitiator. The GelMA solutions were sterilized by filtering through the 0.22 μm filter. GelMA hydrogels were formed by treating the precursor solution with 405 nm ultraviolet (UV) light (25 mW/cm^2) for 20 s. To prepare the GelMA-rhCol3 bioinks, a predetermined amount of type III recombinant human collagen powder (the National Center for Biotechnology Information GenBank Access Number: EF376007, kindly provided by the Bioengineering Lab of Nanjing University of Science and Technology, China) was mixed with the GelMA solutions and stirred for 1 h until fully dissolved. The mixtures were then filtered through 0.22 μm filters and collected in lightproof universal tubes for further use. The composite bioinks prepared in this study were differentiated corresponding to the concentration of rhCol3 while fixing the GelMA concentration at 7.5 wt%. The composite bioinks were named GelMA-rhCol3 – 0.8, 1.6, and 3.2 corresponding to the concentration of rhCol3 (0.8, 1.6, and 3.2 wt%) within the bioinks.

2.2. Cell culture

HaCaTs cell line and human dermal fibroblasts (HDFs) were purchased from the National Infrastructure of Cell Line Resource (NICR, Beijing). The HaCaTs and HDFs were cultured in Dulbecco's Modified Eagle Medium (DMEM; Wisent, Canada) supplemented with 10% fetal bovine serum (Gibco, Beijing), 1% GlutaMax (Gibco, Beijing), 1% non-essential amino acids (Gibco, Beijing), and 1% penicillin-streptomycin (Gibco, Beijing). The cells were passaged before reaching a confluence of 80 – 90%, with the culture medium changed every other day when culturing at 37°C and 5% CO_2. For HaCaTs cultured on hydrogels in 24-well transwell inserts (Thermo Fisher Scientific, Denmark), the culture medium was

supplemented with an additional 1.5 mM $CaCl_2$ under the submerged condition for the initial cell attachment and expansion. To induce the HaCaTs differentiation under the ALI culture condition, the submerged culture medium was further supplemented with 50 μg/mL ascorbic acid (Sigma-Aldrich, USA) and 10 ng/mL keratinocyte growth factor (KGF; Lonza, USA).

2.3. Cell viability assay

To visualize the distribution and survival of the HDFs encapsulated in the gelled bioinks, we applied a LIVE/DEAD™ (Invitrogen, USA) assay at defined time points (days 1, 3, and 7). Briefly, cell-laden samples were gently washed 3 times with warm phosphate-buffered saline (PBS), then 500 μL LIVE/DEAD™ staining solution (Calcein-AM 2 μmol/L, PI 4.5 μmol/L) was added, followed by incubation at 37°C for 20 min. The fluorescent images were taken by confocal fluorescent microscopy (Eclipse Ti Nikon), and cell viability was determined by identifying the number of live and dead cells using Matrix Laboratory (MATLAB R2019a). Viabilities of printed HDFs in different photocrossslinked bioinks were evaluated in the same manner. In addition, a LIVE/DEAD™ assay was also used to identify the seeded HaCaTs on the surface of bioinks.

2.4. Cell proliferation assay

To determine the suitable concentration of the bioink, we prepared GelMA solutions at varying concentrations (5, 7.5, and 10 wt%) encapsulated with 1×10^6/mL HDFs. At a defined culture time point, the culture medium was removed, and fresh medium supplemented with Cell Counting Kit-8 (CCK-8, Yeason Biotechnology, China) reagent (mixing ratio of 10:1) was added to the individual sample followed by a 3 h culturing at 37°C. A 100 μL of the reacted supernatant was then transferred to a 96-well plate from each sample, and the optical density was measured at an absorbance wavelength of 450 nm (Multiskan FC Thermo). To determine the proliferation activities of the HDFs within the dermal constructs or HaCaTs proliferated on hydrogel constructs, dermal constructs or epidermal layers were treated with the same method.

2.5. Quantitative real-time polymerase chain reaction (PCR)

The gene expression levels of collagen I, TGF-β, vimentin, and alpha-smooth muscle actin (α-SMA) were measured using qRT-PCR. After culturing for 14 days, cell-laden hydrogels were dissolved by GelMA lysis solution (EFL-Gm-Ls-001), then HDFs were isolated from the dissolved bioinks by centrifugation. The cells were lysed by Trizol® for 5 min to obtain the total RNA of the fibroblasts cultured in bioink hydrogels. To determine the effects of rhCol3 on the gene expressions (P63, filaggrin, and Nrf2) of HaCaTs, we cultured HaCaTs on GelMA-rhCol3-3.2 and GelMA only hydrogels and performed qRT-PCR analysis. At defined culture time points (days 1, 3, and 7), the HaCaTs on the surface of the dermal constructs were gently washed with PBS and detached by trypsin. The detached HaCaTs were then lysed by Trizol® for 5 min to obtain cell suspension. After centrifuging the cell suspensions at 12×10^3 rpm for 5 min, the supernatants were collected, followed by the addition of chloroform to collect the RNA-containing aqueous phase. Isopropanol was then added to the aqueous phase, which was centrifugated to obtain the RNA pellets. Finally, the RNA pellets were dissolved in RNase-free water. The first-strand cDNA was synthesized using OneScript Plus cDNA Synthesis Kit (Applied Biological Materials Inc., Richmond, BC, Canada) with 1000 ng total RNA. The PCR reaction was performed in a StepOnePlus Real-Time PCR System (Applied Biosystems, Foster City, CA, USA) following the instructions from EvaGreen qPCR MasterMix (Applied Biological Materials Inc., Richmond, BC, Canada). The $2^{-\triangle\triangle Ct}$ method was used to determine the relative mRNA expression levels, and all the results were normalized to the expression of β-actin. The primers sequences for the target genes are listed in **Table S1**.

2.6. Scanning electron microscope (SEM)

The hydrogel samples were lyophilized firstly for 24 h; then, the freeze-dried samples were carefully sectioned using a scalpel and sputter coated for 60 s with gold. The microstructure morphology of the samples was observed by SEM (FEI Quanta 200, Netherlands) at an acceleration voltage of 5 kV. The average pore size was determined by measuring the diameter of randomly selected pores.

2.7. Rheology and mechanical characterizations

The rheological properties of the GelMA and the GelMA-rhCol3 composite bioinks were evaluated by a rheometer (Anton Paar Mcr-302) with a 25 mm plate (CP 25-2/TG). The storage modulus (G') and loss modulus (G'') of the inks were determined under the temperature sweep mode by decreasing the temperature from 37°C to 4°C at a cooling rate of 5°C/min while the shear strain and frequency were maintained at 0.5% and 1 Hz, respectively. The photorheological properties of the GelMA and the GelMA-rhCol3 composite bioinks were evaluated by a rheometer (Anton Paar Mcr-302) equipped with a transparent glass plate with Peltier control (Anton Paar, P-PTD 200GL) and a 25 mW/cm^2 UV light source. The storage modulus (G') and loss modulus (G'') of the

inks were determined along with the testing time up to 900 s under a constant temperature of 37°C, while the shear strain and frequency were maintained at 0.5% and 1 Hz, respectively. The time taken for the initial storage modulus of each bioink group to reach 50% and 80% of the averaged storage modulus at the post-UV crosslinking stage was also determined to illustrate the photo crosslinking efficiency.

To evaluate the effect of GelMA and rhCol3 concentration on the mechanical properties of the gelled bioinks, the compressive modulus of the hydrogels was determined by compression test in this study. The square-shaped samples with 14.5 mm side length and 4.5 mm height were prepared and compressed up to 50% strain at the rate of 2 mm/min using a mechanical test instrument (Bose ElectroForce 3200, Bose Corp.). The compressive modulus was determined from the initial linear slope (10 – 15% strain) of the stress-strain curves.

2.8. Printability characterization

The printability was assessed by a filament fusion test consisting of printing parallel strands at decreasing spacing, according to a previous study[30]. The initial filament distance was set to 2.5 mm, decreased 0.1 mm for each subsequent line, and ended at the distance of 0.3 mm. The printing head and the collecting platform of the bioprinter (Biomaker 2, SunP Biotech) were set to 23 and 10°C, respectively. The printing speed of the nozzle was 2 mm/s, and the extrusion speed was 0.3 mm^3/s; a 25G extrusion needle was selected in the test. The printed parallel strands were cross-linked by a 405 nm light source for 20 s to form gelled construct and photos recorded by a digital camera. The fused filament length (*fs*) at each edge of the meandering pattern to their corresponded filament thickness (*ft*) was determined and plotted for each filament distance (*fd*). Lattice structures were also printed out to assess the printability (Pr value) of the bioinks based on a well-established approach[31]. Pr denotes value of printability that is defined based on square shape using the following equation: $Pr=L^2/16A$, where L and A denote the perimeter and the area of the square, respectively.

2.9. rhCol3 dissolution test

To quantify the releasing of the rhCol3 from the gelled bioinks, rhCol3 was conjugated with fluorescent dye. Predetermined rhCol3 and NHS-fluorescein were fully dissolved in PBS to prepare the 10 wt% and 0.6 wt% solutions, respectively. The prepared solutions were then mixed and stirred at 37°C for 3 h in dark room. The well-mixed solution was then diluted with four volumes of PBS and transferred to dialysis bag (MW.14000) to dialyze the unreacted fluorescent dye for 14 days. The final dialyzed solution was then freeze-dried to obtain the fluorescent-labeled rhCol3. The rhCol3-contained hydrogels were then prepared and incubated in PBS. The 500 μL PBS was collected from each sample and the same amount of fresh PBS was added. The time to collect the PBS was set to 1 h, 3 h, 5 h, 10 h, 1 d, 3 d, 5 d, 10 d, and 14 d after initial incubation in a 37°C incubator. The fluorescent intensity was determined by a microplate reader (Molecular Devices, SpectraMax M2) at excitation wavelength of 494 nm and emission wavelength of 518 nm.

2.10. Engineering human skin equivalent in transwell inserts

To create human dermal constructs in transwell inserts, the line distance of the model was adjusted to 0.1 mm, and the printing shape was changed to round to adapt the 24-well transwell. Bioinks that contained 1×10^6/mL HDFs were prepared and then transferred into a 3 mL syringe equipped with a 25G extrusion needle before printing. A 405 nm UV light was used to crosslink the construct immediately after printing. A 200 μL fresh medium was added into the transwell insert followed by placing the transwell into a 24-well plate that contained 500 μL medium. The printed dermal layer constructs were cultured for 3 days before seeding the HaCaTs on their upper surface at a density of 2×10^5 cells/cm^2. They were cultured with submerged medium for another 5 days, followed by switching to the ALI medium while lifting the insert to a level where the HaCaTs contact the air, allowing for an ALI culture condition for HaCaTs. Both the submerged medium and ALI medium were changed every other day. The attached areas of proliferated HaCaTs were imaged with microscopy at days 3 and 6 until the cells reached full confluence and the percentage of the cover area was determined by Matrix Laboratory (MATLAB R2019a). LIVE/DEAD™ staining assay was also applied to identify the proliferation of the HaCaTs on dermal surfaces.

2.11. Skin equivalent characterizations

The printed skin constructs were harvested from the transwell insert at week 3 and week 6 since the initial culture or ALI culture. The skin constructs were fixed with 4% paraformaldehyde for 20 min at room temperature before paraffin embedding. They were then cut into sections and mounted onto slides for hematoxylin and eosin (H&E) staining. For immunohistochemistry staining, the sections were deparaffinized and rehydrated with xylene and ethanol and were immersed in EDTA antigen retrieval buffer, followed by blocking with 3% BSA for 30 min. The slides were then incubated overnight at 4°C in a humid chamber, with primary antibodies against cytokeratin 14 (1:100, Abcam) and cytokeratin

10 (1:100, Abcam). After washing with PBS 3 times with 10 min between each wash, we added secondary antibodies (goat-anti-mouse antibody 1:300 and goat-anti-rabbit antibody 1:400, Servicebio) and incubated the sections for 1 h at room temperature followed by PBS washing 3 times. Finally, the slides were counterstained with DAPI for 10 min at room temperature and then washed with PBS 3 times before observation under a confocal microscope. The K14 and K10 fluorescent intensity levels of the immunohistochemistry sections were quantitatively analyzed using FIJI software.

2.12. *In vivo* experiment

Eight-week-old SD rats were used, and all animal experiments were performed according to the protocols approved by the National Institutes of Health Guide for the Care and Use of Laboratory Animals, China. All experiments and procedures were approved by Laboratory Animal Research Center, Tsinghua University (SYXK 2019-0037). Intraperitoneal injection of 10% chloral hydrate (3 mg/kg) was applied to anesthetize the rat. Then, the hairs on the dorsal surface were shaved, and the skin was sterilized with 75% alcohol. Full-thickness excisional wounds were created on the back of each rat by a 5 mm diameter biopsy punch. Bioinks were then carefully added to the trauma through injection, which was followed by UV crosslinking to gel the inks. Wounds without any treatment were set as controls. All samples were carefully covered with medical gauze and secured with Tegaderm™ dressing (3M Health Care, Germany) immediately to protect them from dryness and self-grooming damage. At days 3, 7, and 14 after the operation, photos of wound sites were taken, and the wound areas were determined using Matrix Laboratory (MATLAB R2019a). To determine the healing progress, we sacrificed all rats at day 14 and carefully excised wound sites with the surrounding skin. About 4% paraformaldehyde was used to fix the tissues overnight, and later, the tissues were dehydrated in graded ethanol and embedded in paraffin. The embedded block was sectioned with 10 μm of thickness and stained with H&E and Masson's trichrome (MT) staining (Beyotime Institute of Biotechnology, China). Images of the H&E-stained tissue were taken with microscopy (Eclipse TS100 Nikon) for further study.

2.13. Statistical analysis

Unless otherwise stated, the data are presented as the mean ± standard deviation with triplicate or more for each condition throughout this study using GraphPad Prism 6. Statistical significance was assessed with a Student's *t*-test, and significance was indicated with $*P < 0.05$, $**P < 0.01$, and $***P < 0.001$, where $P \geq 0.05$ was considered not statistically significant.

3. Results and discussion

3.1. Determining the suitable concentration of GelMA for engineering the *in vitro* dermal constructs

We first optimized the concentration of GelMA, the base bioink content, regarding the construction of the dermal layer. We encapsulated HDFs in GelMA hydrogels at varying concentrations (5, 7.5, and 10 wt%) and evaluated the activity of HDFs *in vitro*. The LIVE/DEAD™ staining indicated that HDFs viability in all groups was maintained over 90% throughout the 7-day culture (**Figure 2A**). The majority of HDFs presented a spherical morphology at day 3 among all groups while displaying a more elongated spreading morphology at day 7 (**Figure 2A**). The CCK-8 assay revealed the proliferation of HDFs, and we found that 7.5 wt% GelMA supported a significantly higher growth rate at day 7 (**Figure 2B**), which was 1.3 and 1.5 fold of those obtained by 5 and 10 wt% GelMA, respectively. This is in accordance with the previous studies reporting that cellular processes are highly affected by physical cues provided by the surrounding ECM[32]. As supporting evidence, SEM images of lyophilized GelMA hydrogels demonstrated that the pore size decreased with the increase of GelMA concentration (**Figure 2C and Figure S1**), in agreement with the previous studies[33]. It should be noted that such microporosity in the lyophilized state does not represent the nanoporosity generated by cross-linked polymer mesh in the hydrogel state[34]. The stiffness of the GelMA hydrogels has been found to be another crucial parameter in regulating the proliferation of the HDFs. The mechanical compression tests demonstrated that 10 wt% GelMA showed much higher compression modulus (22.6 kPa) than 7.5 and 5 wt% GelMA did (7.5 and 3.5 kPa, respectively) (**Figure S2**). Too stiff hydrogel has been demonstrated to hinder cell activity, while too soft hydrogel might face challenges in supporting prolonged cell growth[35,36]. Similar to our results, a recent study reported that, compared to 5 and 10 wt% GelMA hydrogel, HDFs cultured in 7.5 wt% GelMA hydrogel showed the highest proliferation activities[37]. Another study revealed increased remodeling and proliferation activities in the 5 wt% GelMA group compared to GelMA hydrogels (10 and 15 wt%) with much higher stiffness[38].

We further investigated the gene expression of HDFs cultured in 5, 7.5, and 10 wt% GelMA hydrogels. Particularly, the expression of relevant genes, such as type I collagen (Col-I), TGF-β, vimentin, and α-SMA, was examined by PCR analysis after culturing for 14 days (**Figure 2D**). Col-I is the fundamental ECM structure protein that plays critical roles, such as supporting and maintaining the integrity of the dermal architecture in skin tissue[39]. TGF-β and vimentin are known as

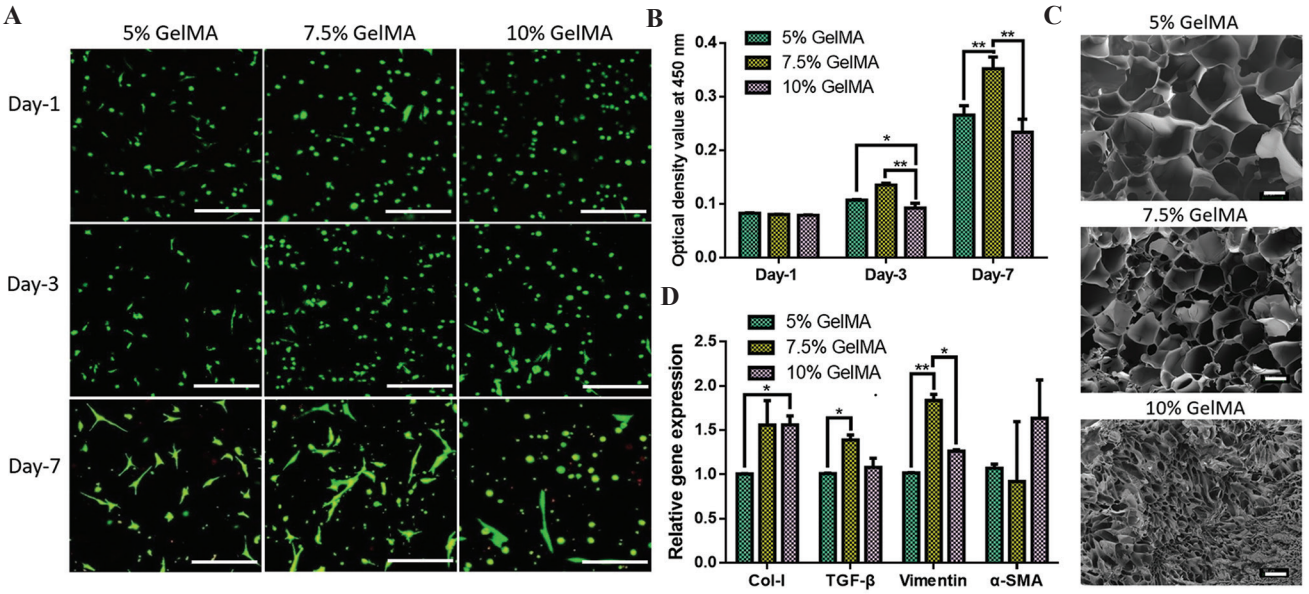

Figure 2. Optimizing the base component in the bioink for the 3D bioprinting of the *in vitro* dermal constructs. (A) LIVE/DEAD™ staining of proliferated HDFs within 5, 7.5, and 10 wt% GelMA during 7-day culture. Scale bars: 50 μm. (B) Quantification of the proliferation activities of the HDFs in GelMA hydrogels using CCK-8 assay. Significance is indicated with $*P < 0.05$ and $**P < 0.01$, n = 3. (C) SEM images of lyophilized hydrogels, showing the microporous morphology. Scale bars: 100 μm. (D) Gene expressions of the skin ECM-associated proteins within 5, 7.5, and 10 wt% GelMA. Significance is indicated with $*P < 0.05$ and $**P < 0.01$, $n = 3$.

critical factors that regulate the cell fate of fibroblasts; for instance, TGF-β could induce the secretion of ECM proteins while vimentin has been found in coordinating fibroblast proliferation and keratinocyte differentiation in skin tissue[40,41]. In addition, α-SMA is known to be involved in stress fiber formation and transition of fibroblast to myofibroblast, hence, its gene expression level was also determined[42]. The results showed that HDFs cultured in 7.5 and 10 wt% GelMA expressed higher level of Col-I than HDFs cultured in 5 wt% GelMA (**Figure 2D**). Expressions of TGF-β and vimentin from 7.5 wt% GelMA group were found higher than those of 5 and 10 wt% GelMA groups. There was no significant difference among three groups for the expression of α-SMA. Similar trends on expression of the Col-I and α-SMA have been reported by literature where hydrogels with stiffness comparable to ours have been used[43,44]. These results illustrated that 7.5 wt% GelMA could comprehensively support the cellular activities of the encapsulated skin fibroblasts; therefore, it was selected in constructing the *in vitro* dermis.

3.2. Assessing the rheology and printability of the bioinks

Before bioprinting, we investigated the rheology of bioinks as it critically affects the printability for extrusion-based bioprinting. To determine the thermosensitivity of the GelMA-rhCol3 composite bioinks with various rhCol3 concentrations, we performed an oscillatory temperature sweep from 37 to 4°C. The results indicated that both storage (G') and loss (G'') moduli of all tested samples increased rapidly in the range of 14 – 22°C, with a significantly higher G' than G'' beyond this region while cooling (**Figure 3A**). In contrast, rhCol3 alone with concentration up to 3.2 wt% presented low G' and G'' (<1 Pa) throughout the temperature range (**Figure S3**). These results evidenced the thermal gelation of GelMA-rhCol3 composite bioinks, which is likely due to the consistent presence of GelMA. Meanwhile, the results also showed that adding rhCol3 would induce a slightly decreased modulus and gelation temperature; the G' at 4°C and gel transition temperature for GelMA-rhCol3 bioink containing 3.2 wt% rhCol3 (termed GelMA-rhCol3-3.2) were ~1.1 kPa and ~16°C, respectively, while those for GelMA alone bioink were ~1.9 kPa and ~18°C (**Figure 3A and S4**). To further investigate the effect of rhCol3 on photocrosslinking kinetics, we performed photorheological time sweep tests and assessed the change of G' than G'' with the *in situ* UV irradiation during the testing (**Figure 3B**). All tested samples show a rapid increase of G' on UV irradiation. After approximately 100 s of irradiation, the G' became gradually plateaued, indicating that the photocrosslinking reaction approached the end. The UV exposure time durations that allowed G' reach 50% and 80% of the plateaued modulus were determined and shown in **Figure S5A**. It took the GelMA-rhCol3-3.2 group significantly shorter time than others to achieve

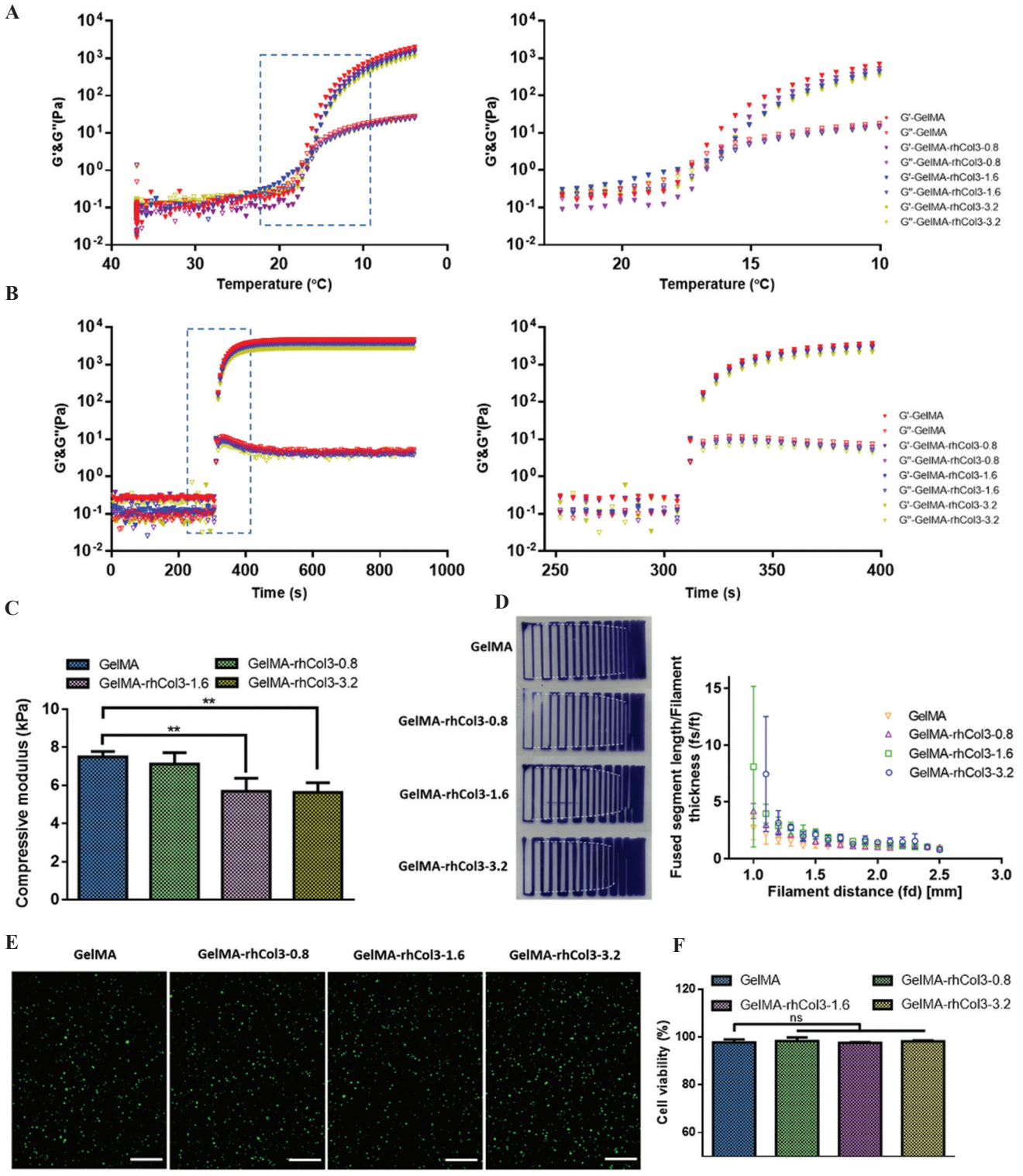

Figure 3. Assessing the rheology and printability of the bioinks. (A) Storage and loss moduli of the bioinks determined by an oscillatory temperature sweep from 37 to 4°C. (B) Storage and loss moduli of the bioinks determined during photocrosslinking at 37°C. (C) Compressive modulus of the photocrosslinked hydrogels with varied rhCol concentrations. Significance is indicated with $*P < 0.05$ and $**P < 0.01$, no significance is indicated with ns, $n = 3$. (D) Filament fusion test of the bioinks (pictures of printed constructs) and plot of fused filament length (*fs*) normalized by filament thickness (*ft*) as a function of the filament distance (*fd*) of the tested bioinks. (E) LIVE/DEAD™ fluorescent staining images of the printed HDFs in different bioinks post-photocrosslinking and (F) quantitative cell viability of the printed dermal constructs 1 h after printing. Scale bars: 50 μm.

the same degree of crosslinking. Similar to the thermal gelation experiment, we found that plateaued G' decreased with the increase of rhCol3 concentration; rhCol3-free sample (GelMA) possessed the highest G' (~4.5 kPa) at its equilibrium, while the plateaued G' of GelMA-rhCol3-3.2 was only ~3.0 kPa (**Figure S5B**). The compression test further confirms the effect of rhCol3 on the mechanical properties of the composite bioinks after gelation. As shown in **Figure 3C**, the compressive modulus decreased with the increase of rhCol3 concentration in the 7.5 wt% GelMA; the compressive moduli of GelMA-rhCol3-3.2 (~5.6 kPa) and GelMA-rhCol3-1.6 (~5.7 kPa) were significantly lower than that of plain GelMA (~7.5 kPa). Collectively, the inclusion of rhCol3 in GelMA would slightly slow down the kinetics of thermal and photogelation, as well as the mechanical properties after gelation. This is probably because the soluble free rhCol3 chains would interrupt the helix formation of GelMA and chain growth photopolymerization. Similar results were reported in the literature, where decreased G' was observed for GelMA/Alginate or GelMA/collagen hydrogels after adding non-cross-linked alginate or collagen, respectively[45,46].

To evaluate the shape fidelity of our bioinks, we performed a filament fusion test using an approach adapted from the literature[30]. Briefly, fused segment length (*fs*) of parallel printed strands to their corresponded filament thickness (*ft*) was determined for varied filament distance (*fd*) (**Figure 3D**). The results indicated that the *fs* value increased with the decrease of *fd* in all tested groups. Meanwhile, adding rhCol3 into the GelMA led to a slight increase of *fs*. As a result, *fs/ft* of GelMA-rhCol3-3.2 was higher than those of other groups at selected *fd*. Using another printability assessment approach that characterizes the circularity of the micropores in a printed structure[31], we utilized the optimized temperatures for different formulations while obtaining similar printability of Pr values that were close to 1. Lower printing temperature (~18°C) is needed for GelMA-rhCol3-3.2 compared to that of GelMA (~21°C) (**Figure S6**). These findings are associated with the rheological results that the presence of additional rhCol3 reduces the G'.

We fluorescently labeled rhCol3 and quantified the release of rhCol3 at different initial concentrations from photocrosslinked GelMA. The results (**Figure S7**) demonstrated a burst release of rhCol3 in the beginning (~30% at day 1) and a plateau after 1 week (~70% of release). Since the soluble rhCol3 could not be properly cross-linked without additional chemical modification, the major retaining mechanisms are likely the physical trapping and physical interaction with GelMA network. Nevertheless, the rhCol3 is still presenting throughout the culturing period, and nearly 30% will be stably maintained in the formulation after 2 weeks.

Apart from printability and collagen dissolution test, we assessed the cell viability post-printing using different bioink formulations. The LIVE/DEAD™ staining results showed homogeneous HDFs distribution within the printed constructs and high cell viability (~97%) (**Figure 3E and F**), which further confirmed the feasibility of constructing the dermal layer using 3D bioprinting and GelMA-rhCol3 bioinks.

3.3. Evaluating the proliferation activities of HDFs and HaCaTs

To determine the effect of rhCol3 on the growth of HDFs, we bioprinted HDFs-laden dermal constructs using different bioink formulations and performed a CCK-8 assay during a 14-day culture. The results indicated that the embedded HDFs proliferated in both GelMA control and GelMA-rhCol3 composite bioink over time. All the tested groups yielded similar HDFs proliferation rates, and adding rhCol3 to the GelMA did not reduce the proliferation activities compared to the control group (**Figure 4A**).

We then examined the effect of rhCol3 on the growth of upper seeded HaCaT cells (**Figure 4B**). It showed that the cell activities at day 3 were significantly higher than those at day 1, indicating the growth of cells. It also showed that the proliferation was accelerated by adding rhCol3 to the bioinks as GelMA group possessed the lowest optical density (OD) value at days 1 and 3. After culturing for 5 days, there was no significant difference among all tested samples, suggesting that the HaCaTs cells became confluent on top of dermal constructs (**Figure 4B**). We also performed an epidermal keratinocytes migration assay to assess the formation of the epidermal layer (**Figure 4C**). To indicate the acellular area, white circles were used to label the uncovered region and images are shown in **Figure S8**. After 3 days of culture, the coverage percentage shifted to a higher number (~98%) with the inclusion of rhCol3 to the bioinks than that ~80% of rhCol3-free counterpart (**Figure 4D**). After culturing for 5 days, the HaCaTs monolayers imaged from all tested samples show nearly confluent status with no significant difference (**Figure 4D**). This is likely due to the continuous proliferation and migration of HaCaTs on the GelMA-based dermis layer, confirmed by the literature[47]. Nevertheless, these results demonstrated that rhCol3 facilitated HaCaTs adhesion, proliferation, and migration; therefore, the rhCol3-contained composite bioinks should have the potential of supporting epidermis development and regeneration.

We further evaluated the influence of rhCol3 on the HaCaTs gene expression using PCR analysis (**Figure 4E**). We found that the mRNA level of the gene P63, which regulates both the proliferation and differentiation of epidermal keratinocytes[48], increased

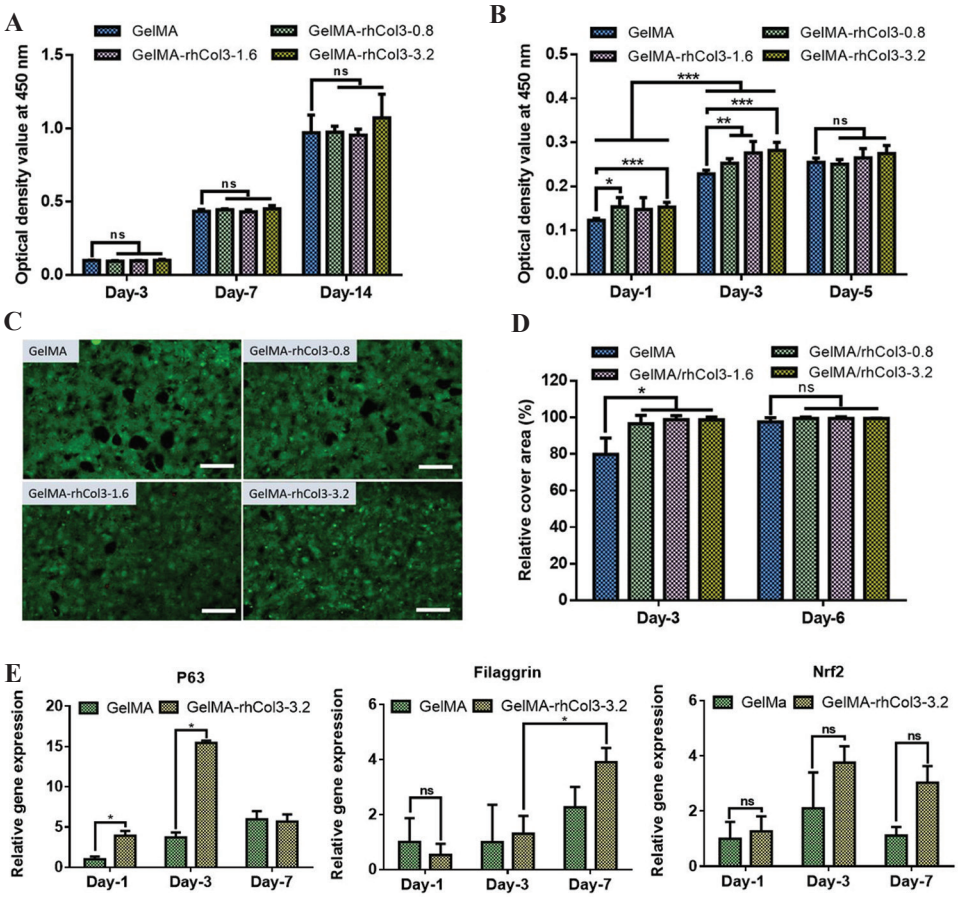

Figure 4. Proliferation activities of HDFs and HaCaTs in printed dermal constructs. (A) Quantified proliferation of the HDFs within the dermal constructs and (B) optical density value of seeded HaCaTs on top of the dermal constructs at different time points. Significance is indicated with $*P < 0.05$, $**P < 0.01$, and $***P < 0.001$, no significance is indicated with ns, $n = 3$. (C) LIVE/DEAD™ fluorescent images of the cell monolayers developed on dermal constructs at day 3. Scale bars: 200 μm. (D) Relative cover area formed by proliferated HaCaTs at days 3 and 6. Significance is indicated with $*P < 0.05$, none significance is indicated with ns, $n = 3$. (E) Gene expressions of P63, filaggrin, and Nrf2 in epidermal layers of GelMA-rhCol3-3.2 bioinks and the GelMA group. Significance is indicated with $*P < 0.05$, $n = 3$.

significantly at day 3 in both GelMA and the GelMA-rhCol3-3.2 groups. This suggests that our *in vitro* skin construct models the initial stage of epidermis repair and regeneration, in which the proliferation and regeneration of keratinocytes play a crucial role. Interestingly, P63 expression in the GelMA-rhCol3-3.2 group was 3-fold of that in GelMA control group at day 3 and day 1, indicating that rhCol3 significantly affects HaCaTs at an early stage. This is probably because the rhCol3 promotes HaCaTs proliferating and spreading before covering the full area of the attached substrate. The gene expression of filaggrin, a gene associated with the HaCaTs differentiation and the epidermal barrier function[49], increased significantly after 1 week of culture in both GelMA and GelMA-rhCol3-3.2 groups, while the expression in the GelMA-rhCol3-3.2 group was 1.25-fold of that in the GelMA group. This was likely because the HaCaTs differentiation occurred later than proliferation, though both proliferation and differentiation progressed at an early stage. The gene expression of Nrf2 that responds to oxidative stress was also examined, and we found that at days 3 and 7, the expression of Nrf2 in the GelMA-rhCol3 group reached 1.8-fold and 2.7 fold of that in the rhCol3-free group. This result suggests that our skin construct based on GelMA-rhCol3 bioink could mimic skin repair and regeneration process, evidenced by the previous study that has validated the role of Nrf2 in regulating cellular stresses during wound healing[50,51].

3.4. Histological examination and immunohistochemistry study of the fabricated skin constructs

Next, we evaluated the formation of epidermis supported by underlying dermis composited with different bioinks formulations. We sectioned the fabricated skin constructs at week 6 and stained them with H&E. The staining

images indicated that our 3D-printed skin constructs possessed both proliferative basal and differentiated upper epidermis, with the basal proliferated HaCaT appearing to be denser, which represented tissue histology similar to that of native human skins (**Figure 5A**). We further quantified the thickness of the epidermis layer under different conditions and found that there were no significant differences of the epidermis thickness, the average thickness ranged from 37 to 41 μm throughout the tested bioink formulations (**Figure 5B**). The *in vitro* skin constructs were generated from basal HaCaT epidermal cell proliferation and differentiation, which was supported by a biomimetic tissue microenvironment generated by our composite bioinks.

We further conducted immunohistochemistry of the skin constructs to detect the epidermal keratinocyte cell markers, keratin 14 (K14) and keratin 10 (K10) at week 3 and week 6. Marker K14 typically indicates HaCaTs in proliferation status, while K10 indicates a higher potential of differentiation. **Figure 5C** shows that our skin construct

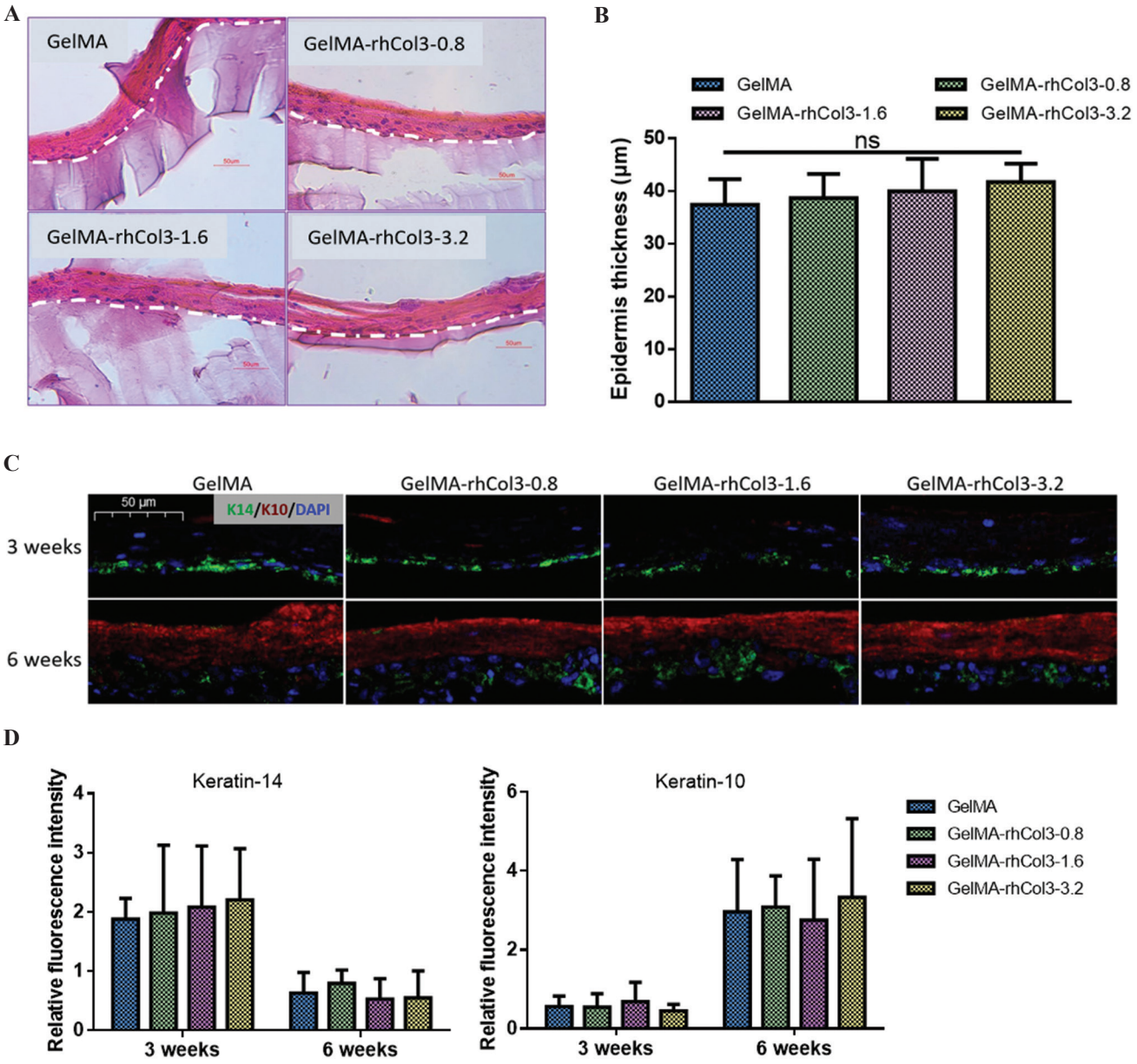

Figure 5. Histological examination of the prepared skin constructs and immunohistochemistry study of the epidermal layer. (A) H&E staining images of the epidermal layers of the *in vitro* skin constructs after 6 weeks of ALI culture, with the barrier of the epidermal layer (upper) to the bioprinted dermal constructs indicated with dotted lines. Scale bars: 50 μm. (B) Epidermis thickness of the skin constructs (n = 3). (C) Immunohistochemistry images of the epidermal layers on skin constructs showing merged DAPI (blue), K14 (green), and K10 (red). Scale bar: 50 μm. (D) Fluorescent intensity of the expression of the K14 and K10 from epidermal layers at weeks 3 and 6.

had functional basal HaCaTs expressing proliferative marker K14 at week 3, while the differentiation marker K10 was seldom observed. This is probably because the *in vitro* skin constructs were at an early stage of differentiation under ALI condition (3 weeks since the ALI culture). In contrast, differentiation marker K10 was significantly detected at week 6 in all groups, indicating that the *in vitro* skin construct formed a more differentiated upper epidermal layer. The fluorescent intensity of the marker K14 and K10 was quantified and is shown in **Figure 5D**. There were no significant differences in the intensity among the tested groups, suggesting that the fabricated *in vitro* skin constructs supported the differentiation activities of the HaCaTs and formed epidermal layers with uniform structures.

3.5. *In vivo* evaluation of bioinks

To further explore the feasibilities of using composite bioinks containing rhCol3 to the *in vivo* skin repair and regeneration, we developed a full-thickness skin defect model of SD rats. The GelMA-rhCol3-3.2 and GelMA were selected to treat the skin wounds by depositing hydrogel precursors on the wounded site followed by *in situ* photocrosslinking. The skin tissue repair and regeneration were evaluated by measuring wound closure rate and by examining the histological staining.

Figure 6A shows the wound closure process at different time points after puncturing at day 0. The biological replicates of wound closure experiments are supplied in **Figure S9**. We converted the wounded area

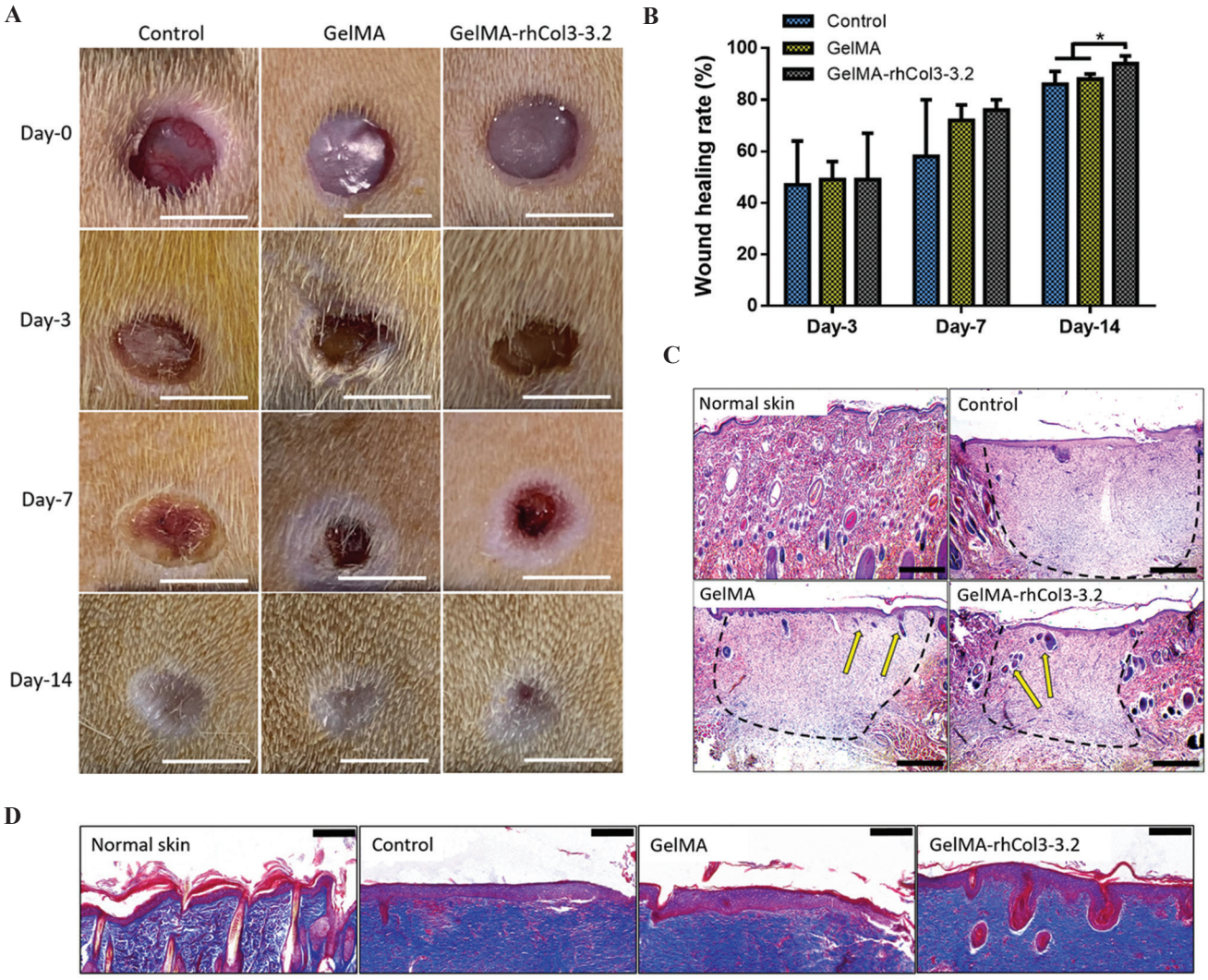

Figure 6. Closure of wounds treated with different bioinks. (A) Representative photographs of hydrogel-treated wounds at days 0, 3, 7, and 14. Scale bars: 5 mm. (B) The quantitative wound healing rates of the tests. Significance is indicated with $*P < 0.05$, $n = 3$. (C) H&E staining images of wound sections, with wound areas and new growth of hair follicles indicated with black dotted lines and yellow arrows, respectively. Scale bars: 500 μm. (D) Masson's trichrome staining images of regenerated epidermal layers compared to normal skin. Scale bars: 200 μm.

to a quantitative wound healing rate at each time point shown in **Figure 6B**. There was no significant difference in the wound area among groups at day 3 and day 7, although GelMA-rhCol3-3.2 group seemed to yield a slightly higher healing rate at day 7. However, by day 14, the healing rate of GelMA-rhCol3-3.2 group (~94%) was significantly higher than those of GelMA-only and blank control groups (**Figure 6B**). H&E staining further revealed the skin regeneration of the wound sites at day 14 (**Figure 6C**). Fresh hair follicles were also found in the regenerated dermis of GelMA-rhCol3-3.2 group. The regenerated epidermal layers and collagen deposition within the wounds were further stained with Masson's trichrome (**Figure 6D)**. Compared to the native skin tissue of the SD rat, thicker regenerated epidermal layers were found in both GelMA and GelMA-rhCol3-3.2 group, and GelMA-rhCol-3.2 group showed freshly regenerated hair follicles located right underneath the new epidermis. In addition, collagen depositions were found in all wounds as collagen fibers were stained in blue by the Masson's trichrome. Similar to our findings, it has been recently reported that the human collagen facilitates the proliferation and migration of mouse fibroblasts by stimulating skin regeneration relevant growth factors, and further influences the repairing of the mouse skin defects[7]. The mechanical properties of the hydrogels might also affect the *in vivo* outcome. Since GelMA-rhCol3-3.2 has lower stiffness compared to GelMA group, it might be easier for the proliferated fibroblasts to penetrate into the softer hydrogel and replace it with the newly formed tissue.

4. Conclusion

Biomaterials that support wound healing and skin regeneration are long needed. In this study, we introduced the rhCol3 as a novel bioink component and systematically investigated its role in skin tissue engineering. We first selected 7.5 wt% GelMA as a base bioink formulation based on an optimization of the 3D culture of HDFs. Further, we formulated a series of GelMA-rhCol3 composite bioinks by varying the rhCol3 concentrations (from 0.8 to 3.2 wt%) and achieved desirable printability and cell viability (~90%) with extrusion-based bioprinting. The mechanical properties, rheologies, and printabilities of the composite bioinks were carefully investigated, and we found that the addition of rhCol3 to the GelMA led to a decrease in hydrogel stiffness, storage modulus, and likely printability. Later, we successfully built a human skin equivalent (epidermis layer of around 40 μm in thickness) using our bioink and bioprinting technique. The *in vitro* study suggested that adding rhCol3 to the GelMA would enhance the proliferation of keratinocytes in the epidermal layers at the early stage of culture. The addition of rhCol3 was further proven to upregulate the expression levels of the key genes relevant to the proliferation and differentiation of HaCaTs. The inclusion of rhCol3 in the GelMA bioink contributed to the faster wound healing *in vivo*, though no significant increase of epidermis thickness was observed *in vitro*. Overall, rhCol3 could be used as a potential biomaterial to improve the skin tissue microenvironment and thus for the general skin tissue engineering applications. Future studies will pay more attention to the signaling pathways regulated by the bioink composites during skin tissue regeneration.

Acknowledgments

The authors acknowledge the Bioengineering Lab of Nanjing University of Science and Technology for the kind gift of rhCol3. The authors also acknowledge Prof. Ting Zhang and Prof. Jiabin Guo for the initial discussion on the project.

Funding

The authors acknowledge the funding support from the National Natural Science Foundation of China (No. 52105306), Higher Education Discipline Innovation Project (111 Project, No. B17026), Tsinghua University Initiative Scientific Research Program (No. 20197050024), and New Faculty Start-up Funding provided by Tsinghua University (012-53330200421).

Conflict of interest

The authors declare no conflicts of interest.

Author contributions

Conceptualization: Yang Yang, Wei Sun and Liliang Ouyang
Data curation: Yang Yang and Runze Xu
Funding acquisition: Wei Sun and Liliang Ouyang
Investigation: Yang Yang, Runze Xu, Chengjin Wang and Yuzhi Guo
Project administration: Wei Sun and Liliang Ouyang
Supervision: Wei Sun and Liliang Ouyang
Validation: Yang Yang and Runze Xu
Visualization: Yang Yang and Runze Xu
Writing (original draft): Yang Yang and Runze Xu
Writing (review & editing): Yang Yang and Runze Xu

Ethics approval and consent to participate

All experiments and procedures were approved by Institutional Animal Care and Use Committee, Tsinghua University (F16-00228; A5061-01).

References

1. Kanitakis J, 2002, Anatomy, histology and immunohistochemistry of normal human skin. *Eur J*

Dermatol, 12:390–9.

2. Gonzales KA, Fuchs E, 2011, Skin and its regenerative powers: An alliance between stem cells and their niche. *Dev Cell*, 43:387–401. https://doi.org/10.1016/j.devcel.2017.10.001
3. Fuchs E, Raghavan S, 2002, Getting under the skin of epidermal morphogenesis. *Nat Rev Genet*, 3:199–209. https://doi.org/10.1038/nrg758
4. Watt FM, Huck W, 2013, Role of the extracellular matrix in regulating stem cell fate. *Nat Rev Mol Cell Biol*, 14:467–73. https://doi.org/10.1038/nrm3620
5. Chung JH, Seo JY, Choi HR, *et al.*, 2001, Modulation of skin collagen metabolism in aged and photoaged human skin *in vivo*. *J Invest Dermatol*, 117:1218–24. https://doi.org/10.1046/j.0022-202x.2001.01544.x
6. D'Hondt S, Guillemyn B, Syx D, *et al.*, 2018, Type III collagen affects dermal and vascular collagen fibrillogenesis and tissue integrity in a mutant Col3a1 transgenic mouse model. *Matrix Biol*, 70:72–83. https://doi.org/10.1016/j.matbio.2018.03.008
7. Guo Y, Bian Z, Xu Q, *et al.*, 2021, Novel tissue-engineered skin equivalent from recombinant human collagen hydrogel and fibroblasts facilitated full-thickness skin defect repair in a mouse model. *Mater Sci Eng C Mater Biol Appl*, 130:112469. https://doi.org/10.1016/j.msec.2021.112469
8. Zoppi N, Gardella R, De Paepe A, *et al.*, 2004, Human Fibroblasts with Mutations in COL5A1 and COL3A1 Genes Do Not Organize Collagens and Fibronectin in the Extracellular Matrix, Down-regulate α2β1 Integrin, and Recruit αvβ3 Instead of α5β1 Integrin. *J Biol Chem*, 279:18157–68. https://doi.org/10.1074/jbc.M312609200
9. Epstein EH, 1974, [α1(III)]3 Human Skin Collagen: Release by pepsin digestion and preponderance in fetal life. *J Biol Chem*, 249:3225–31. https://doi.org/10.1016/S0021-9258(19)42661-6
10. Gref R, Deloménie C, Maksimenko A, *et al.*, 2020, Vitamin C-squalene bioconjugate promotes epidermal thickening and collagen production in human skin. *Sci Rep*, 10:16883. https://doi.org/10.1038/s41598-020-72704-1
11. Lovell CR, Smolenski KA, Duance VC, *et al.*, 2010, Type I and III collagen content and fibre distribution in normal human skin during ageing. *Br J Dermatol*, 117:419–28. https://doi.org/10.1111/j.1365-2133.1987.tb04921.x
12. Riekki R, Parikka M, Jukkola A, *et al.*, 2002, Increased expression of collagen Types I and III in human skin as a consequence of radiotherapy. *Arch Dermatol Res*, 294:178–84. https://doi.org/10.1007/s00403-002-0306-2
13. Cheng W, Yan-Hua R, Fang-Gang N, *et al.*, 2011, The content and ratio of type I and III collagen in skin differ with age and injury. *Afr J Biotechnol*, 10:2524–9. https://doi.org/10.5897/AJB10.1999
14. Fuchs E, Blau HM, 2020, Tissue stem cells: Architects of their niches. *Cell Stem Cell*, 27:532–56. https://doi.org/10.1016/j.stem.2020.09.011
15. Yu W, Wang G, Luo X, *et al.*, 2012, Substrate stiffness regulates the proliferation, migration, and differentiation of epidermal cells. *Burns*, 38:414–20. https://doi.org/10.1016/j.burns.2011.09.002
16. Ng MR, Besser A, Danuser G, *et al.*, 2012, Substrate stiffness regulates cadherin-dependent collective migration through myosin-II contractility. *J Cell Biol*, 199:545–63. https://doi.org/10.1083/jcb.201207148
17. Gangatirkar P, Paquet-Fifield S, Li A, *et al.*, 2007, Establishment of 3D organotypic cultures using human neonatal epidermal cells. *Nat Protoc*, 2:178–86. https://doi.org/10.1038/nprot.2006.448
18. Mathes SH, Ruffner H, Graf-Hausner U, 2014, The use of skin models in drug development. *Adv Drug Deliv Rev*, 69-70:81–102. https://doi.org/10.1016/j.addr.2013.12.006
19. Kim BS, Kwon YW, Kong JS, *et al.*, 2018, 3D cell printing of *in vitro* stabilized skin model and *in vivo* pre-vascularized skin patch using tissue-specific extracellular matrix bioink: A step towards advanced skin tissue engineering. *Biomaterials*, 168:38–53. https://doi.org/10.1016/j.biomaterials.2018.03.040
20. Lee V, Singh G, Trasatti JP, *et al.*, 2014, Design and fabrication of human skin by three-dimensional bioprinting. *Tissue Eng Part C Methods*, 20:473–84. https://doi.org/10.1089/ten.TEC.2013.0335
21. Koch L, Deiwick A, Schlie S, *et al.*, 2012, Skin tissue generation by laser cell printing. *Biotechnol Bioeng*, 109:1855–63. https://doi.org/10.1002/bit.24455
22. Kim BS, Lee JS, Gao G, *et al.*, 2017, Direct 3D cell-printing of human skin with functional transwell system. *Biofabrication*, 9:025034. https://doi.org/10.1088/1758-5090/aa71c8
23. Fertala A, 2020, Three Decades of Research on Recombinant Collagens: Reinventing the Wheel or Developing New Biomedical Products? *Bioengineering (Basel)*, 7:155. https://doi.org/10.3390/bioengineering7040155
24. Yang L, Wu H, Lu L, *et al.*, 2021, A tailored extracellular

matrix (ECM) - Mimetic coating for cardiovascular stents by stepwise assembly of hyaluronic acid and recombinant human Type III collagen. *Biomaterials*, 276:121055. https://doi.org/10.1016/j.biomaterials.2021.121055

25. Fushimi H, Hiratsuka T, Okamura A, *et al.*, 2020, Recombinant collagen polypeptide as a versatile bone graft biomaterial. *Commun Mater*, 1:87. https://doi.org/10.1038/s43246-020-00089-9
26. Huang J, Lei X, Huang Z, *et al.*, 2022, Bioprinted gelatin-recombinant Type III collagen hydrogel promotes wound healing. *Int J Bioprint*, 8:517. https://doi.org/10.18063/ijb.v8i2.517
27. Gelse K, Pöschl E, Aigner T, 2003, Collagens–structure, function, and biosynthesis. *Adv Drug Deliv Rev*, 55:1531–46. https://doi.org/10.1016/j.addr.2003.08.002
28. Zhou F, Hong Y, Liang R, *et al.*, 2020, Rapid printing of bio-inspired 3D tissue constructs for skin regeneration. *Biomaterials*, 258:120287. https://doi.org/10.1016/j.biomaterials.2020.120287
29. Nielsen MJ, Karsdal MA, 2016, Type III collagen. In: Karsdal MA, editor. Biochemistry of Collagens, Laminins and Elastin. Ch. 3. Massachusetts, United States: Academic Press. p21-30.
30. Ribeiro A, Blokzijl MM, Levato R, *et al.*, 2017, Assessing bioink shape fidelity to aid material development in 3D bioprinting. *Biofabrication*, 10:014102. https://doi.org/10.1088/1758-5090/aa90e2
31. Ouyang L, Yao R, Zhao Y, *et al.*, 2016, Effect of bioink properties on printability and cell viability for 3D bioplotting of embryonic stem cells. *Biofabrication*, 8:035020. https://doi.org/10.1088/1758-5090/8/3/035020
32. Bonnans C, Chou J, Werb Z, 2014, Remodelling the extracellular matrix in development and disease. *Nat Rev Mol Cell Biol*, 15:786–801. https://doi.org/10.1038/nrm3904
33. Reis LA, Chiu L, Yan L, *et al.*, 2012, A peptide-modified chitosan–collagen hydrogel for cardiac cell culture and delivery. *Acta Biomater*, 8:1022–36. https://doi.org/10.1016/j.actbio.2011.11.030
34. Ouyang L, Wojciechowski JP, 2022, Tunable Microgel-Templated Porogel (MTP) Bioink for 3D Bioprinting Applications. *Adv Healthc Mater*, 11:e2200027. https://doi.org/10.1002/adhm.202200027
35. Ouyang L, Armstrong JP, Lin Y, *et al.*, 2020, Expanding and optimizing 3D bioprinting capabilities using complementary network bioinks. *Sci Adv*, 6:eabc5529. https://doi.org/10.1126/sciadv.abc5529
36. Ouyang L, 2022, Pushing the rheological and mechanical boundaries of extrusion-based 3D bioprinting. *Trends Biotechnol*. 40:891–902. https://doi.org/10.1016/j.tibtech.2022.01.001
37. Barros NR, Kim HJ, Gouidie MJ, *et al.*, 2021, Biofabrication of endothelial cell, dermal fibroblast, and multilayered keratinocyte layers for skin tissue engineering. *Biofabrication*, 13:035030. https://doi.org/10.1088/1758-5090/aba503
38. Shie MY, Lee JJ, Ho CC, *et al.*, 2020, Effects of Gelatin Methacrylate Bio-ink Concentration on Mechano-Physical Properties and Human Dermal Fibroblast Behavior. *Polymers (Basel)*, 12:1930. https://doi.org/10.3390/polym12091930
39. Martin P, 1997, Wound healing - Aiming for perfect skin regeneration. *Science*, 276:75–81. https://doi.org/10.1126/science.276.5309.75
40. Fang C, Yue S, Mohanasundaram P, *et al.*, 2016, Vimentin coordinates fibroblast proliferation and keratinocyte differentiation in wound healing via TGF-β–Slug signaling. *Proc Natl Acad Sci U S A*, 113:E4320–7. https://doi.org/10.1073/pnas.1519197113
41. Kwon EJ, Park EJ, Yu H, *et al.*, 2018, SIRT-1 regulates TGF-β-induced dermal fibroblast migration via modulation of Cyr61 expression. *Connect Tissue Res*, 59:245–54. https://doi.org/10.1080/03008207.2017.1360293
42. Baranyi U, Winter B, Gugerell A, *et al.*, 2019, Primary Human Fibroblasts in Culture Switch to a Myofibroblast-Like Phenotype Independently of TGF Beta. *Cells*, 8:721. https://doi.org/10.3390/cells8070721
43. Ibañez RI, do Amaral RJ, Reis RL, *et al.*, 2021, 3D-Printed Gelatin Methacrylate Scaffolds with Controlled Architecture and Stiffness Modulate the Fibroblast Phenotype towards Dermal Regeneration. *Polymers (Basel)*, 13:2510. https://doi.org/10.3390/polym13152510
44. Chester D, Lee V, Wagner P, *et al.*, 2022, Elucidating the combinatorial effect of substrate stiffness and surface viscoelasticity on cellular phenotype. *J Biomed Mater Res A*, 110:1224–37. https://doi.org/10.1002/jbm.a.37367
45. Aldana AA, Valente F, Dilley R, *et al.*, 2021, Development of 3D bioprinted GelMA-alginate hydrogels with tunable mechanical properties. *Bioprinting*, 21:e00105. https://doi.org/10.1016/j.bprint.2020.e00105
46. Ha JH, Lim JH, Kim JW, *et al.*, 2021, Conductive GelMA–Collagen–AgNW Blended Hydrogel for Smart Actuator. *Polymers (Basel)*, 13:1217.

https://doi.org/10.3390/polym13081217

47. Zhao X, Lang Q, Yildirimer L, *et al.*, 2016, Photocrosslinkable Gelatin Hydrogel for Epidermal Tissue Engineering. *Adv Healthc Mater*, 5:108–18. https://doi.org/10.1002/adhm.201500005
48. Koster MI, Roop DR, 2004, The role of p63 in development and differentiation of the epidermis. *J Dermatol Sci*, 34:3–9. https://doi.org/10.1016/j.jdermsci.2003.10.003
49. Proksch E, Brandner JM, Jensen JM, 2008, The skin: An indispensable barrier. *Exp Dermatol*, 17:1063–72. https://doi.org/10.1111/j.1600-0625.2008.00786.x
50. Braun S, Hanselmann C, Gassmann MG, *et al.*, 2002, Nrf2 transcription factor, a novel target of keratinocyte growth factor action which regulates gene expression and inflammation in the healing skin wound. *Mol Cell Biol*, 22:5492–505. https://doi.org/10.1128/MCB.22.15.5492-5505.2002
51. Yin Y, Peng H, Shao J, *et al.*, 2021, NRF2 deficiency sensitizes human keratinocytes to zinc oxide nanoparticles-induced autophagy and cytotoxicity. *Environ Toxicol Pharmacol*, 87:103721. https://doi.org/10.1016/j.etap.2021.103721

Publisher's note